J|A|C|S
ARTICLES
Published on Web 03/11/2003

Pore Formation by 6-Ketocholestanol in Phospholipid Monolayers and Its Interpretation by a General Nucleation-and-Growth Model Accounting for the Sigmoidal Shape of Voltage-Clamp Curves of Ion Channels

Lucia Becucci, Maria Rosa Moncelli, and Rolando Guidelli*

Contribution from the Department of Chemistry, Florence University, Sesto Fiorentino (Florence) 50019, Italy

Received November 21, 2002; E-mail: guidelli@unifi.it

Abstract: 6-Ketocholestanol (KC), a steroid that differs from cholesterol mainly by the presence of a carbonyl group, forms pores inside a dioleoylphosphatidylcholine monolayer self-assembled on mercury by a mechanism similar to that of channel-forming peptides and proteins. The potential steps responsible for pore formation by KC molecules give rise to potentiostatic charge vs time curves whose sigmoidal shape and potential dependence can be quantitatively interpreted on the basis of a mechanism of nucleation and growth of KC clusters. Pore formation by KC allows the penetration of thallous ions across the otherwise impermeable phosphatidylcholine monolayer, while pore disruption taking place at more negative potentials causes a drop in thallous ion permeation. Pore disruption is also accounted for by a mechanism of nucleation and growth of holes inside the KC clusters. The kinetic model of nucleation and growth is general, and accounts quantitatively for the sigmoidal shape and potential dependence of the classical Hodgkin-Huxley voltage-clamp curves of potassium channels in squid giant axon,[1] using a minimum number of free parameters.

Introduction

Channels formed by the so-called channel-forming peptides, such as alamethicin and melittin, are generally regarded as a bundle of membrane-spanning α-helices surrounding a central pore.[2] One face of the helix is hydrophobic, whereas the other is hydrophilic due to the presence of carbonyl groups. The hydrophobic faces are directed outward, so as to establish favorable interactions with the hydrocarbon tails of the lipid bilayer. The hydrophilic faces are directed inward, making the polar residues available for favorable interactions with permeant ions and/or water molecules. A similar model is also assumed for channel forming proteins, such as potassium and sodium channels, whose molecular weight of about 250 000 D is 2 orders of magnitude greater than that of channel forming peptides. Due to their much simpler structure, channel forming peptides are often viewed as models of channel-forming proteins.

Several channel-forming peptides and proteins exhibit sigmoidal potentiostatic current−time curves, that is "voltage-clamp" curves. Thus, the polyene-like antibiotic monazomycin shows typical sigmoidal voltage-clamp curves,[3,4] which were interpreted on the basis of a standard chemical kinetic formulation under the assumption that monazomycin entry into and exit from the membrane is autocatalytic.[5] Sigmoidal voltage-clamp curves were reported for alamethicin-doped membranes at a pressure of 1000 atm;[6] they were also observed at atmospheric pressure,[7] but only over times very short compared to those required to develop the full response to a voltage step. In this case the sigmoidal shape was interpreted by a three-state model in which a nonconducting surface state is followed by a nonconducting precursor state, and then by a conducting state.[8] Among the channel-forming proteins yielding sigmoidal voltage-clamp curves, by far the most familiar are undoubtedly the potassium channels of the squid giant axon investigated by Hodgkin and Huxley,[1] who developed an empirical kinetic description of these curves. Other proteins yielding sigmoidal voltage-clamp curves are the voltage-gated proton channels.[9,10] Their behavior was interpreted on the basis of a model in which protonation at an externally accessible site of the channel stabilizes the closed channel conformation, whereas its deprotonation allows a conformational change resulting in a protonation site exposed to the internal solution, whose protonation stabilizes the open conformation.[11]

Phospholipid self-assembled monolayers on mercury electrodes have been extensively investigated for their applications as models of biological membranes. Molecules of biological

(1) Hodgkin, A. L.; Huxley, A. F. *J. Physiol*. **1952**, *117*, 500−544.
(2) Sansom, S. P. *Prog. Biophys. Mol. Biol*. **1991**, *55*, 139−235.
(3) Muller, U. R.; Finkelstein, A. *J. Gen. Physiol*. **1972**, *60*, 263−284.
(4) Muller, U. R.; Orin, G.; Peskin, C. S. *J. Gen. Physiol*. **1981**, *78*, 171−200.
(5) Muller, R. U.; Peskin, C. S. *J. Gen. Physiol*. **1981**, *78*, 201−229.
(6) Bruner, L. J.; Hall, J. E. *Biophys. J*. **1983**, *44*, 39−47.
(7) Mauro, A.; Nanavati, R. P.; Heyer, E. *Proc. Natl. Acad. Sci. U. S. A*. **1972**, *69*, 3742−3744.
(8) Bruner, L. J. *J. Theor. Biol*. **1985**, *117*, 265−276.
(9) DeCoursey, T. E.; Cherny, V. V. *Biophys. J*. **1996**, *71*, 182−193.
(10) Cherny, V. V.; DeCoursey, T. E. *J. Gen. Physiol*. **1999**, *114*, 819−838.
(11) Cherny, V. V.; Markin, V. S.; DeCoursey, T. E. *J. Gen. Physiol*. **1995**, *105*, 861−896.

10.1021/ja029428j CCC: $25.00

importance,[12−16] lipophilic ions,[17] peptides and proteins [18−20] and channel-forming peptides [21,22] have been incorporated in Hg-supported phospholipid monolayers with the aim of investigating their behavior in an environment mimicking that of biological membranes. These monolayers have the hydrocarbon tails directed toward the hydrophobic mercury surface and the polar heads directed toward the solution.[23] They have a high mechanical stability, a high resistance to electric fields and a notable reproducibility. Over the potential range from −0.2 to −0.8 V versus the saturated calomel electrode (SCE) they behave like a half-membrane. Thus, they are impermeable to inorganic ions and their differential capacity is about 1.7 μF cm^{-2}, namely twice that of black lipid membranes (BLMs). As long as interactions with foreign molecules do not extend beyond the hydrocarbon tail region facing the mercury surface, no appreciable differences between mercury-supported monolayers and BLMs are expected.

This work aims at showing that a very simple hydrophobic molecule such as 6-ketocholestanol (KC), a steroid that differs from cholesterol mainly by the presence of a carbonyl group, may form pores inside a dioleoylphosphatidylcholine (DOPC) monolayer self-assembled on mercury by a mechanism similar to that of channel forming peptides and proteins. The potential steps responsible for pore formation by KC molecules give rise to potentiostatic charge vs time curves whose sigmoidal shape and potential dependence can be quantitatively interpreted on the basis of a mechanism of nucleation and growth of KC clusters. It will also be shown that the same mechanism accounts quantitatively for the sigmoidal shape and potential dependence of the classical Hodgkin−Huxley voltage-clamp curves of potassium channels in squid giant axon,[1] using a minimum number of free parameters.

Materials and Methods

The water used for all experiments was obtained from light mineral water by distilling it once, and by then distilling the resulting water from alkaline permanganate, while discarding the heads. DOPC was obtained from Lipid Products (South Nutfield, Surrey, England). KC from Aldrich was used without further purification. Tetramethylammonium chloride (TMACl) from Fluka and methanol (spectroscopic grade) from Merck were used as received. Merck reagent grade potassium chloride were baked at 500 °C before use to remove any organic impurities.

The homemade hanging mercury drop electrode employed in the measurements, the cell and the detailed procedure to produce self-organized lipid monolayers deposited on mercury are described elsewhere.[24−26] The surface area of the mercury drop was 1.4×10^{-2} cm^2. Differential capacity measurements were carried out using a Metrohm Polarecord E506 (Herisau, Switzerland). The ac signal had a 10 mV amplitude and a 75 Hz frequency. The system was calibrated using a precision capacitor. All potentials were measured versus a saturated calomel electrode (SCE) and are referred to this electrode. The chronocoulometric procedure employed to measure potentiostatic charge vs time curves makes use of a wholly computerized apparatus[27] and is described elsewhere.[17] The microprocessor used to control all the operations was a Model NOVA 4X from Data General (Westboro, Massachussetts), whereas an Amel Model 551 (Milano, Italy) fast rise potentiostat with a rise time 0.1 ms was employed for the potentiostatic control of the three-electrode system. The detailed scheme of the homemade electronic current integrator working under microprocessor control is described in Carlá et al.[28]

Each chronocoulomogram consisted in a series of consecutive potential jumps of progressively increasing height from a fixed initial value E_i, which was usually set equal to −0.200 or −0.250 V, to progressively more negative final values E, and was recorded on a single lipid-coated mercury drop. The charge $Q(t,E)$ following each potential jump $E_i \rightarrow E$ was recorded versus the time t elapsed from the instant of the jump for 100 ms, after which the potential was stepped back to E_i, where it remained for 3 s. This rest time at E_i was sufficient to restore the initial conditions. The curves of the differential capacity C of the lipid monolayers deposited on mercury were constantly measured against the applied potential E following the recording of each chronocoulomogram.

Measurements of the interfacial tension γ against potential on mercury coated with DOPC and (DOPC+KC) monolayers in aqueous 5×10^{-3} and 0.1 M TMACl were carried out by measuring the charge density $Q(t = 100$ ms,$E)$ following potential jumps from −0.450 V, which is the potential of zero charge of aqueous TMACl on uncoated mercury,[29] to progressively varying final potentials E ranging from −0.250 to −1.850 V. The charge following a potential jump from −0.450 to −1.850 V on uncoated mercury, as measured by the chronocoulometric technique, amounts to -23.2 ± 0.1 μC cm^{-2}. This is the charge density, σ_M, at −1.850 V not only on uncoated mercury, but also on an initially DOPC− or (DOPC+KC)-coated mercury electrode, in view of the complete desorption of the lipid film at this potential.[30] The $Q(E)$ vs E curves obtained on lipid-coated mercury were therefore converted into σ_M vs E curves by shifting them along the charge axis so as to set $Q(E = -1.850$ V) equal to -23.2 μC cm^{-2}. The σ_M vs E curves so obtained were then integrated over the applied potential E from −1.850 V backward. In view of the Lippmann equation, $d\gamma = -\sigma_M\, dE$, the integrated curves are plots of $\gamma(E)$-γ(1.850 V) versus E.

(12) Herrero, R.; Tadini Buoninsegni, F.; Becucci, L.; Moncelli, M. R. *J. Electroanal. Chem.* **1998**, *445*, 71−80.
(13) Herrero, R.; Moncelli, M. R.; Guidelli, R.; Carlá, M.; Arcangeli, A.; Olivotto, M. *Biochim. Biophys. Acta* **2000**, *1466*, 278−288.
(14) Moncelli, M. R.; Becucci, L.; Nelson, A.; Guidelli, R. *Biophys. J.* **1996**, *70*, 2716−2726.
(15) Moncelli, M. R.; Herrero, R.; Becucci, L.; Guidelli, R. *Biochim. Biophys. Acta* **1998**, *1364*, 373−384.
(16) Nelson, A. *J. Electroanal. Chem.* **1992**, *335*, 327−343.
(17) Moncelli, M. R.; Herrero, R.; Becucci, L.; Guidelli, R. *J. Phys. Chem.* **1995**, *99*, 9940−9951.
(18) Lecompte, M. F.; Miller, I. R. *Biochemistry*. **1980**, *19*, 3434−3438.
(19) Lecompte, M.-F.; Bras, A.-C.; Dousset, N.; Portas, I.; Salvayre, R.; Ayrault-Jarrier, M. *Biochemistry.* **1998**, *37*, 16 165−16 171.
(20) Miller, I. R.; Bach, D.; Teuber, M. *J. Membrane Biol.* **1978**, *39*, 49−56.
(21) Nelson, A. *Biophys. J.* **2001**, *80*, 2694−2703.
(22) Becucci, L.; Moncelli, M. R.; Guidelli, R. *Biophysical J.* **2002**, *82*, 852−864.
(23) Nelson, A.; Benton, A. *J. Electroanal. Chem.* **1986**, *202*, 253−270.
(24) Moncelli, M. R.; Becucci, L.; Guidelli, R. *Biophys. J.* **1994**, *66*, 1969−1980.
(25) Becucci, L.; Moncelli, M. R.; Herrero, R.; Guidelli, R. *Langmuir* **2000**, *16*, 7694−7700.
(26) Moncelli, M. R.; Becucci., L. *J. Electroanal. Chem.* **1997**, *433*, 91−96.
(27) Foresti, M. L.; Moncelli, M. R.; Guidelli, R. *J. Electroanal. Chem.* **1980**, *109*, 1−14.
(28) Carlá, M.; Sastre de Vicente, M.; Moncelli, M. R.; Foresti, M. L.; Guidelli, R. *J. Electroanal. Chem*. **1988**, *246*, 283−296.
(29) Kimmerle, F. M.; Ménard, H. *J. Electroanal. Chem*. **1974**, *54*, 101−121.
(30) Tadini Buoninsegni, F.; Becucci, L.; Moncelli, M. R.; Guidelli, R. *J. Electroanal. Chem.* **2001**, *500*, 395−407.

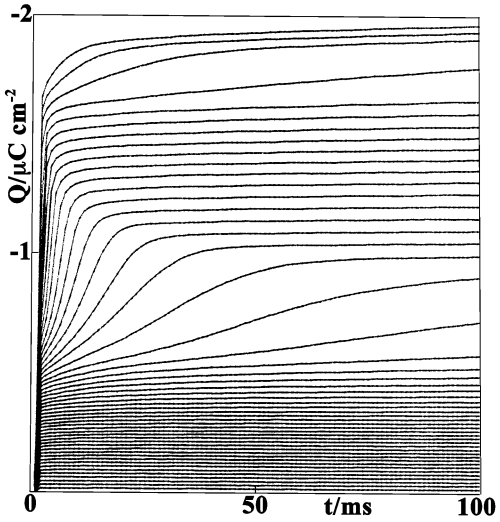

Figure 1. $Q(t,E)$ vs t curves following a series of potential jumps from a fixed initial potential $E_i = -0.250$ V to final potentials E varying by -10 mV increments from -0.250 to -0.750 V on a mercury electrode coated with a lipid monolayer consisting of 67 mol % DOPC + 33 mol % KC and immersed in aqueous 0.1 M KCl.

Results

Figure 1 shows a series charge versus time curves following a series of potential jumps from $E_i = -0.250$ V to progressively more negative potentials E on a mercury electrode coated with a lipid monolayer consisting of 67 mol % DOPC and 33 mol % KC and immersed in aqueous 0.1M KCl. At the less negative final potentials the charge *Q(t,E)* increases abruptly in less than one millisecond, due to the flow of the capacitive current that is required to charge the lipid monolayer, and then remains constant in time. This time-independent charge increases linearly with the applied potential. Subsequently, over a narrow range of final potentials, *Q(t)* increases in time first abruptly, due to the initial capacitive contribution, and then more slowly but more extensively, exhibiting a typical sigmoidal shape that denotes a two-dimensional (2D) phase transition. With a further negative shift in the final potential E, the rate of the phase transition increases causing the charge to attain rapidly a time-independent limiting value, which increases linearly with the applied potential. Then, at still more negative potentials, a second less pronounced 2D phase transition takes place. This is characterized by charge vs time curves exhibiting a roughly linear section before reaching asymptotically a time-independent value. The rate of this further phase transition also increases with a negative shift in the applied potential, causing the charge to attain rapidly a time-independent limiting value, which increases linearly with a negative shift in the applied potential.

Plotting the charge *Q(t)* at a constant time $t = 100$ ms against potential yields two sigmoidal curves separated by three linear segments, whose slopes measure the differential capacity before, between, and after the two phase transitions (curve *a* in Figure 2). The differential capacity C before the first phase transition amounts to 1.2 μF cm^{-2} (see Figure 3) and is therefore lower than that, 1.7 μF cm^{-2}, of a pure DOPC monolayer. The differential capacity between the two phase transitions is appreciably higher, being about equal to 6.5 μF cm^{-2}, whereas that after the second phase transition equals 1.8 μF cm^{-2}. The peculiar rectangular shape of the C versus E curve in Figure 3, due to the two subsequent phase transitions, is not present in the C versus E curves obtained by replacing KC with cholesterol; in the latter case the differential capacity remains constant and about equal to 1.2 μF cm^{-2} over the whole potential range from -0.200 to -0.800 V. Two sigmoidal $Q(t = 100$ s,$E)$ vs E curves analogous to those in Figure 2 are also clearly distinguishable at KC concentrations in the lipid monolayer as low as 12 mol %, just as *Q(t)* vs t curves of sigmoidal shape analogous to those in Figure 1 (data not shown). The height of these curves increases progressively with an increase in KC concentration.

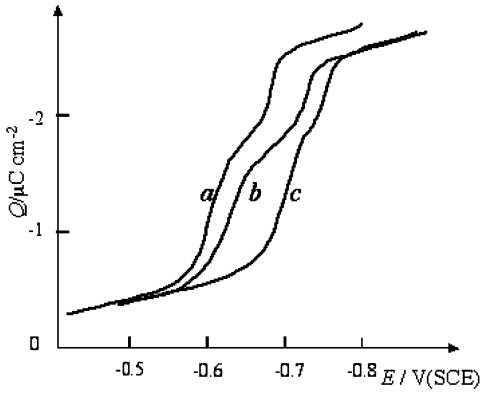

Figure 2. $Q(t = 100$ ms,$E)$ vs E curves on (67 mol % DOPC+33 mol % KC)-coated mercury in aqueous 0.1 (a), 1×10^{-2} (b), and 1×10^{-3} M KCl (c). Here and in the following figures $Q(t,E)$ denotes the charge at time t following a potential jump from $E_i = -0.250$ V to E.

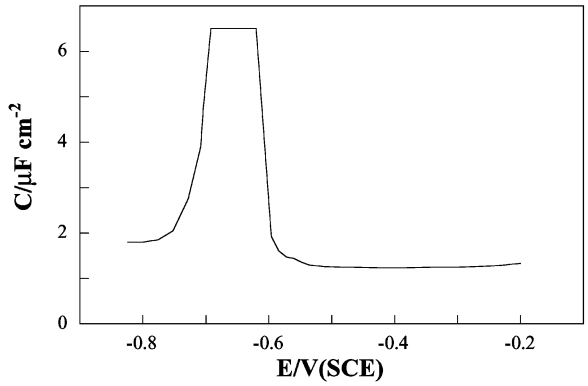

Figure 3. Plot of the differential capacity C versus E on (67 mol % DOPC+33 mol % KC)-coated mercury in aqueous 0.1 M KCl.

The charge vs potential curve at $t = 100$ ms shifts toward more positive potentials with an increase in the KCl concentration, as shown in Figure 2. This increase causes a compression of the diffuse layer adjacent to the lipid monolayer, and hence a decrease in the negative potential difference across this layer, i.e., the surface potential ψ. Hence, the same potential difference across the lipid monolayer is attained at a less negative applied potential the higher is the KCl concentration. However, correcting for the surface potential ψ on the basis of the Gouy−Chapman theory accounts quantitatively for the small positive shift of the $Q(t = 100$ ms,$E)$ vs E curve in passing from 1×10^{-2} to 0.1 M KCl, but not for the positive shift in passing from 5×10^{-3} to 1×10^{-2} M. In fact, this is about 45 mV greater than predicted by the Gouy−Chapman theory. The correction was made by measuring the charge density σ_M on (DOPC+KC)-coated mercury at potentials immediately preceding the rising section of the sigmoidal charge vs potential curve for the first 2D phase transition, and by applying the Gouy−Chapman expression for ψ as a function of σ_M and of the concentration of a 1,1-valent electrolyte.

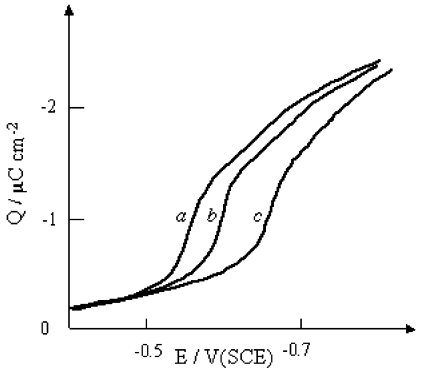

Figure 4. $Q(t = 100$ ms,$E)$ vs E curves on (67 mol % DOPC+33 mol % KC)-coated mercury in aqueous 0.1 (a), 1×10^{-2} (b), and 1×10^{-3} M TMACl (c).

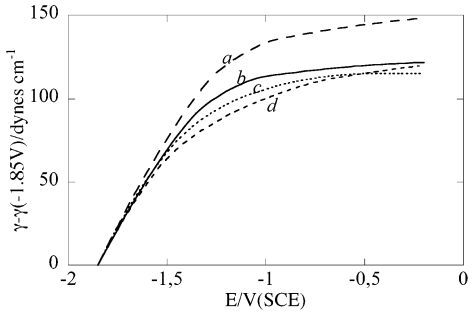

Figure 5. Plots of the interfacial tension γ(E)-$\gamma(-1.85$ V) against E on DOPC-coated mercury in 0.1 M (a) and 5×10^{-3} M TMACl (b), and on (67 mol % DOPC+33 mol % KC)-coated mercury in 0.1 M (c), and 5×10^{-3} M TMACl (d).

A similar behavior is exhibited by the charge vs potential curves obtained using tetramethylammonium (TMA) chloride in place of KCl under otherwise identical conditions, as shown in Figure 4. Here, the passage from the first to the second phase transition is much more blurred than with KCl. Moreover, upon correcting for the surface potential ψ, the positive shift in passing from 5×10^{-3} to 1×10^{-2} M TMA amounts to 30 mV and is only slightly greater than that, 25 mV, in passing from 1×10^{-2} to 0.1 M TMA. The above behavior strongly suggests an involvement of the electrolyte in the first 2D phase transition induced by KC. Further evidence in support of this conclusion is provided by the interfacial tension γ of the (DOPC+KC) monolayer as compared with that of the DOPC monolayer. Figure 5 shows that on DOPC-coated mercury γ increases in passing from 5×10^{-3} to 0.1 M TMACl throughout the whole potential range investigated. Conversely, on (DOPC+KC)-coated mercury this trend is reversed at potentials positive of -0.500 V.

The two phase transitions undergone by the mixed DOPC−KC monolayer have a marked effect on the electroreduction of thallous ion on mercury with thallium amalgam formation. The electroreduction of 10^{-4} M Tl^+ on bare mercury yields a charge vs potential curve characterized by Nernstian electron transfer and diffusion control,[22,31] as shown by curve *a* in Figure 6.

Conversely, no reduction current of thallous ion is observed at a mercury electrode coated with a pure DOPC monolayer up to -0.8 V, when the DOPC film starts to become permeable to inorganic ions (curve *c* in Figure 6). The presence of KC in the lipid monolayer causes Tl^+ electroreduction to take place over

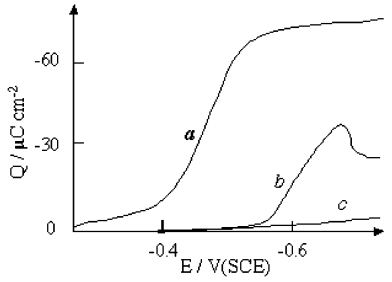

Figure 6. $Q(t = 100$ ms,$E)$ vs E plots for the electroreduction of 1×10^{-4} M Tl^+ from aqueous 0.1 M KCl on bare mercury (a), on (67 mol % DOPC+33 mol % KC)-coated mercury (b), and on DOPC-coated mercury (c).

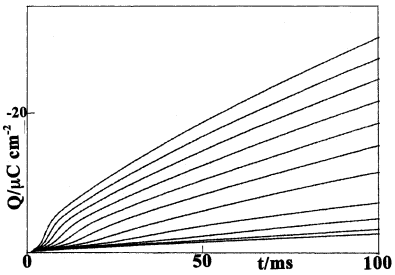

Figure 7. $Q(t,E)$ vs t curves for the electroreduction of 1×10^{-4} M Tl^+ from aqueous 0.1 M KCl following a series of potential jumps from a fixed initial potential $E_i = -0.250$ V to final potentials E varying by -10 mV increments from -0.550 to -0.650 V on (67 mol % DOPC + 33 mol % KC)-coated mercury.

the potential range of the first phase transition, as shown by curve *b* in Figure 6. The resulting charge vs potential curve is now controlled by Tl^+ translocation across the potential energy barrier created by the lipid film. When the faradaic charge becomes greater than about one tenth of the diffusion limiting charge on bare mercury, this curve is also partially controlled by diffusion. At potentials corresponding to the second 2D phase transition the charge due to Tl^+ reduction drops abruptly, denoting an appreciable decrease in film permeability to this cation.

Figure 7 shows the potentiostatic charge vs time curves for Tl^+ electroreduction over the whole potential range of the first phase transition. These curves exhibit a sigmoidal shape that parallels that of the curves of the mixed DOPC−KC monolayer in the absence of Tl^+. It should be noted that the charge in the presence of Tl^+ is more than 1 order of magnitude greater than in its absence, and hence must be ascribed to Tl^+ electroreduction induced by the phase transition, and not to the phase transition per se. At electrolysis times *t*, at which the phase transition is complete, the charge in Figure 7 increases linearly in time, thus denoting that the corresponding faradaic current attains a time-independent value.

Discussion

Over the potential range preceding the first 2D phase transition and characterized by a differential capacity as low as 1.2 μF cm^{-2}, the DOPC and KC molecules are expected to be randomly distributed within the monolayer. Under these conditions KC has the same effect as cholesterol in increasing the rigidity of the film and decreasing its differential capacity.[32] The first phase transition must be ascribed to an increase in the alignment of the KC dipoles along the direction of the interfacial

(31) Nelson, A.; Bizzotto, D. *Langmuir* **1999**, *15*, 7031−7039.

(32) Nelson, A.; Auffret., N. *J. Electroanal. Chem.* **1988**, *244*, 99−113.

electric field, with the oxygen of the carbonyl group more fully turned toward the aqueous solution and also, possibly, to a penetration of potassium ions more deeply into the polar-head region of the lipid film. Both charge movements tend to cause a positive shift in the potential difference across the lipid monolayer, as measured from the metal toward the solution. At constant applied potential this shift must, therefore, be compensated for by a flow of electrons to the metal surface along the external circuit. This causes the increase in negative charge that characterizes the 2D phase transition. The notable increase in differential capacity over the potential range between the two phase transitions is to be ascribed to the first phase transition giving rise to pores in the lipid monolayer. Under these conditions, inorganic ions can move back and forth along the pores following the a.c. signal, causing an increase in differential capacity. The important role of exposed carbonyl oxygens in forming pores is demonstrated by synthetic apolar analogues of alamethicin. These peptaibols are still permeable to ions thanks to the carbonyl oxygen of the G11 residue, despite the lack of polar side chains.[33,34] The decrease in differential capacity from 6.5 to 1.8 μF cm^{-2} after the second phase transition strongly suggests that this transition involves the disruption of the pores and a return to a random distribution of DOPC and KC molecules within the mixed monolayer.

Clear evidence in favor of pore formation is provided by Tl^+ ion electroreduction across the mixed DOPC−KC monolayer. The permeability of the lipid film to Tl^+ ions induced by the first phase transition and its abrupt decrease induced by the second phase transition point to formation and subsequent disruption of pores across the lipid monolayer. The similarity of the sigmoidal shape of the charge versus time curves for Tl^+ electroreduction with that of the much lower capacitive charge vs time curves for the first 2D phase transition in the absence of Tl^+ ions provides further evidence in favor of pore formation.

Model of Nucleation and Growth. The above behavior can be interpreted quantitatively by a kinetics of nucleation and growth. Clusters of monomeric units (such as single KC molecules) resulting from a series of consecutive collisions are considered to be characterized by a critical size, called nucleus, below which they have a higher tendency to shrink by releasing one unit than to grow by aggregation of a further unit, and above which they have a practically irreversible tendency to increase. We will refer to the formation of this critical size from monomeric units as nucleation, and to the irreversible increase beyond the critical size as growth. Let us denote by θ the fraction of the electrode surface area covered by monomers, by θ_0 its initial value before the start of nucleation and growth, and by p the potential-dependent probability of the monomers being in an orientation favorable to their aggregation into clusters. If we denote by n the number of monomers composing a nucleus, then the elementary step yielding the nucleus consists of the incorporation of a monomer into a (n-1)-meric subcritical cluster. This may result from (n-1) elementary steps consisting in the incorporation of each monomeric unit into the immediately preceding subcritical cluster, starting from an initial monomer acting as a "nucleation center". It may also result from n elementary steps in which the first step consists of the aggregation of a monomer to a nucleation center different from a monomer, which in the present case might be an adsorbed potassium or TMA ion. If we assume that all steps preceding the step yielding the nucleus are in quasi-equilibrium, then the nucleation rate υ_N will be proportional to the nth power of the surface coverage, $p\theta$, by the favorably oriented monomers randomly distributed in the monolayer, according to a nucleation rate constant k_N

$$\frac{dN}{dt} \equiv \upsilon_N = k_N(p\theta)^n \tag{1}$$

Here N is the number of nuclei per unit surface area. If the nucleation center is different from the monomer, then the nucleation rate will also be proportional to the concentration of the nucleation centers.

Assuming for simplicity that the cross-sectional area A of a growing supercritical cluster is a circle of radius R, the rate of growth of A is given by the time derivative of πR^2. Moreover, it is proportional to the frequency of the successful impacts of the favorably oriented random monomers, of surface coverage $p\theta$, with the circumference $2\pi R$ of the cluster, according to a proportionality constant k_R

$$\frac{dA}{dt} = \frac{d}{dt}(\pi R^2) = 2\pi R\frac{dR}{dt} = k_R 2\pi R p\theta \rightarrow \frac{dR}{dt} \equiv \upsilon_R = k_R p\theta \tag{2}$$

It follows that the rate υ_R of radial growth of a supercritical cluster is proportional to $p\theta$ according to the rate constant k_R. It should be stressed that the frequency of the successful impacts is not controlled by the two-dimensional diffusion of the KC monomers within the monolayer, but rather by the occurrence of a favorable mutual orientation of the cluster and of the aggregating monomer.

The ratio S_x of the hypothetical area covered by the growing clusters over that, $p\theta_0$, initially covered by the favorably oriented monomers, if the overlapping of the growing clusters could be ignored is called the "extended area". This is expressed by the general relationship[35]

$$S_x = \int_0^t A(y,t)\upsilon_N(y)dy \tag{3}$$

where $A(y,t)$ is the area of the cluster nucleated at time y and observed at time t. Noting that the area $A(y,t)$ of a circular cluster of radius R is given by

$$A(y,t) = \pi R(y,t)^2 = \pi[\int_y^t \upsilon_R(z)dz]^2 \tag{4}$$

S_x takes the form

$$S_x = \pi\int_0^t [\int_y^t \upsilon_R(z)dz]^2\upsilon_N(y)dy \tag{5}$$

The ratio S of the area actually covered by the growing clusters over that initially covered by the favorably oriented monomers is related to the corresponding hypothetical "extended" area S_x, which neglects cluster overlapping, by Avrami's differential equation[36−38]

$$dS/dt = (1 - S)dS_x/dt \tag{6}$$

(33) Fox, R. O.; Richards, F. M. *Nature* **1982**, *300*, 325−330.
(34) Hall, J. E.; Vodyanoy, I.; Balasubramanian, T. M.; Marshall, G. R. *Biophys. J.* **1984**, *45*, 233−247.
(35) Bosco, I.; Rangarajan, S. K. *J. Electroanal. Chem.* **1981**, *129*, 25−51.

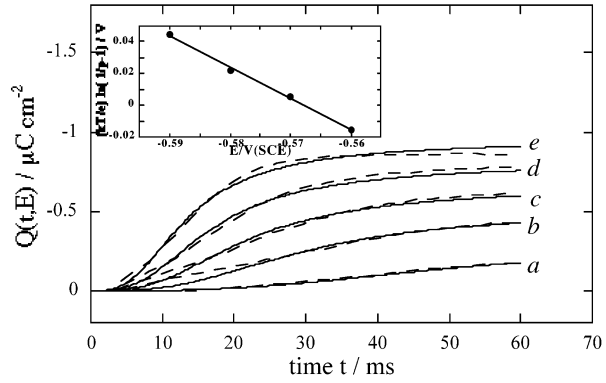

Figure 8. Solid curves are $Q(t,E)$ vs E plots for the first 2D phase transition of a (67 mol % DOPC+33 mol % KC) monolayer self-assembled on mercury, corrected for the capacitive charge passed before the phase transition takes place. E values: −0.560 (a), −0.570 (b), −0.580 (c), −0.590 (d), and −0.600 V (e).The dashed curves were calculated for $n = 2$, $\theta_0 = 0.33$, $\Delta\sigma_M = -2.94\ \mu$C cm^{-2}, $k_N^{1/2}k_R = 6 \times 10^3$ s$^{-3/2}$ and for $p = 0.35$ (a), 0.55 (b), 0.7 (c), 0.85 (d), and 1 (e). The inset shows the corresponding $-(kT/e)\ln(1/p\text{-}1)$ vs E plot.

Substituting the rates of nucleation and of radial growth from eqs 1 and 2 into eq 5 and solving the resulting equation together with eq 6 as outlined in the Appendix yields S as a function of time and of the probability p. The fraction of the electrode surface area covered by the pore-forming clusters is then equal to $p\theta_0 S(t,p)$. It should be noted that the fractional area covered by clusters should by no means be regarded as homogeneous. Rather, it should be regarded as consisting of separate channel-forming aggregates of possibly different size dispersed in the DOPC monolayer.

The fractional surface area $p\theta_0 S(t,p)$ differs from the experimental charge $Q(t,E)$ by a factor equal to the difference $\Delta\sigma_M$ between the charge densities of the metal covered by the clusters and by the random monomers, which can be regarded as independent of potential. Fitting the calculated $\Delta\sigma_M\ p\theta_0 S(t,p)$ vs t curves at different p values to the experimental $Q(t,E)$ vs t curves at different applied potentials E requires three free parameters, apart from the constant normalizing factor $\Delta\sigma_M$. They are the number n of monomers composing a nucleus, the potential-independent product $k_R k_N^{1/2}$, which summarizes the kinetic features of the whole nucleation-and-growth process, and the potential dependent probability p. Thus, identical results are obtained with k_R much lower, equal or much higher than k_N, provided that the $k_R k_N^{1/2}$ product is kept constant. Therefore, this model may account for the formation both of small dispersed clusters, when the rate constant of nucleation is higher than that of radial growth, and of larger aggregates in the opposite case.

Figure 8 shows the experimental $Q(t,E)$ vs t curves at different potentials together with the $p\theta_0 S(t,p)$ vs t curves calculated for $n = 2$, $\Delta\sigma_M = -2.94\ \mu$C cm^{-2}, $k_R k_N^{1/2} = 6 \times 10^3$ s$^{-3/2}$ and for different values of the probability p. The experimental $Q(t,E)$ vs t curves were corrected for the capacitive charge that flows in less than 1 ms from the potential jump, before the first 2D phase transition occurs. The correction was made by measuring the charge from the straight line obtained by extrapolation of the linear section of the Q vs E curve a in Figure 2 that precedes this phase transition. The calculated curves account satisfactorily both for the increase in the height of the sigmoidal curves with an increase in p and for the concomitant shift of the inflection point toward shorter times. Moreover, the probability p depends on the applied potential according to the Boltzmann equation

$$p = \left\{1 + \exp\left[-\frac{ze(E - E_{1/2})}{kT}\right]\right\}^{-1} \qquad (7)$$

Thus, the plot of $-(kT/e)\ln(1/p\text{-}1)$ vs E (see the inset of Figure 8) is linear and exhibits a slope $z = -1.98$, which can be regarded as a "gating charge" in electronic units. In other words, a positive charge of about 2e must move toward the electrode under the action of the applied potential in order to impart to the KC molecules the orientation favorable for the formation of a pore. If this charge were to be ascribed exclusively to an increase in the alignment of the KC dipoles corresponding to an increase $\Delta\mu$ in their dipole-moment normal component, the contribution of one KC molecule to the gating charge should be equal to $\Delta\mu/l$, where l is the average length of the dipole. This is not realistic, because the KC molecules tend to orient the oxygen of their carboxyl group toward the aqueous phase even in the absence of an external field, and hence at potentials positive of those at which the first 2D phase transition occurs.[39] If we assume that the increase in the alignment of the KC dipoles amounts to 30% of their total dipole moment of 3.1 D, about 0.5 nm in length, then the contribution of one KC molecule to the gating charge would be about equal to 0.04e. Thus, if the gating charge were to be ascribed exclusively to a reorientation of KC molecules, a single cluster would consist of about 50 molecules, which is an exceedingly large number. This strongly suggests that the formation of pores also requires the movement of K^+ or TMA ions, acting as nucleation centers, into the polar-head region of the lipid monolayer. A confirmation of the involvement of these supporting cations comes from the positive shift in the charge vs potential curves in Figures 2 and 4 with an increase in electrolyte concentration even upon correction for diffuse layer effects. The enhancing effect of K^+ ions upon pore formation seems to reach saturation already at a concentration of 1×10^{-2} M, while that of TMA ions continues at least up to 0.1M.

Interfacial Tension. A further confirmation of the involvement of the supporting cations comes from the interfacial tension measurements in Figure 5. The electrochemical potential of a monovalent cation incorporated in an insoluble film is given by[40]

$$\tilde{\mu}_+{}^m = \mu_+{}^{0,m} + kT\ln a_+{}^m + e\phi^m - \gamma A_+ \qquad (8)$$

Here $\mu_+{}^{0,m}$ is the standard chemical potential of the ion in the film, $a_+{}^m$ its activity, A_+ its surface area, ϕ^m the electrical potential at the position occupied by the ion and γ the interfacial tension. At equilibrium, $\tilde{\mu}_+{}^m$ is equal to the electrochemical potential of the ion in the bulk solution

$$\tilde{\mu}_+{}^b = \mu_+{}^{0,b} + kT\ln a_+{}^b + e\phi^b \qquad (9)$$

where the superscript b denotes quantities in the bulk solution.

(36) Avrami, M. *J. Chem. Phys.* **1939**, *7*, 1103−1112.
(37) Avrami, M. *J. Chem. Phys.* **1940**, *8*, 212−224.
(38) Avrami, M. *J. Phys. Chem.* **1941**, *9*, 177−184.
(39) Franklin, J. C.; Cafiso, D. S. *Biophys. J.* **1993**, *65*, 289−299.
(40) Defay, R.; Prigogine, I.; Bellemans, A.; Everett, D. H. *Surface Tension and Adsorption*; Longmans, Green & Co: London, UK, 1966; p 210.

Consequently

$$\gamma A_+ = (\mu_+^{0,m} - \mu_+^{0,b}) + kT\ln(a_+^m/a_+^b) + e(\phi^m - \phi^b) \quad (10)$$

On a DOPC-coated electrode the cations do not penetrate deeply into the polar-head region of the film. Hence, an increase in a_+^b is expected to cause a proportional increase in a_+^m in agreement with a linear (Henry) isotherm, leaving the kTln-(a_+^m/a_+^b) term substantially unaltered. On the other hand, this increase compresses the diffuse layer causing the potential difference ($\phi^m - \phi^b$) at the negatively charged electrode to become less negative, with a resulting increase in the interfacial tension γ. Such an increase in γ with an increase in the TMA concentration is indeed observed on DOPC-coated mercury over the whole potential range investigated, as shown in Figure 5, curves *b* and *a*. On (DOPC+KC)-coated mercury at potentials negative of about −0.50 V, TMA ions seem to penetrate more deeply into the polar-head region, thus experiencing a greater portion of the negative potential difference across the whole interface. Therefore, the compression of the diffuse layer caused by the increase in the bulk TMA concentration, a_+^b, has a weaker effect in decreasing the negative value of ($\phi^m - \phi^b$) and in increasing γ, as appears from Figure 5, curves *d* and *c*. In the proximity of −0.50 V, the penetration of the cations into the film becomes more pronounced, with a certain tendency to saturation as the TMA concentration increases. Therefore, the increase in TMA concentration causes the a_+^m/a_+^b ratio to decrease, with the ($\phi^m - \phi^b$) potential difference remaining constant. This causes γ to decrease with an increase in a_+^b in view of eq 10, as actually observed experimentally at potentials positive of −0.50 V.

Movement of Tl^+ Ions along the KC Pores. The curves of the charge density *Q(t,E)* for Tl^+ electroreduction induced by KC pore formation against time and their dependence upon the applied potential can also be interpreted by the present model. These curves develop at potentials negative of the standard potential, −0.463 V/SCE,[22] of the Tl^+/Tl(Hg) couple by more than 130 mV, where the backward electrode reaction can be neglected. Confining ourselves to *Q* values much less than the diffusion-controlled faradaic charge, for which the depletion of Tl^+ ions near the lipid film is negligible, the faradaic charge density Q_b controlled by a charge-transfer step at a bare Hg electrode is expressed by the equation

$$Q_b = Fc_{Tl^+} k\beta^{-1}\left[\exp(\beta^2 t)erfc(\beta t^{1/2}) + \frac{2}{\pi^{1/2}}\beta t^{1/2} - 1\right] \quad with\ \beta = \frac{k}{D^{1/2}} \quad (11)$$

This equation is obtained by integrating the corresponding expression for the faradaic current[41] over time. Here, c_{Tl+} and $D = 2 \times 10^{-5}$ cm^2/s are the bulk concentration and the diffusion coefficient of Tl^+ ion and *k* is the rate constant for the charge-transfer step. The faradaic charge at the Hg electrode coated with the mixed DOPC−KC monolayer is obtained by multiplying the above expression for Q_b by the time-dependent surface coverage, $p\theta_0 S(t,p)$, by the KC pore-forming clusters, as calculated by the present model. The solid curves in Figure 9 are experimental $Q(t,E)$ vs *t* plots for 10^{-4} M Tl^+ electroreduction at three different applied potentials, while the corresponding dashed curves were calculated with the parameters reported in the legend. Agreement between experimental and calculated curves is quite good. The *k* values providing the best fit vary exponentially with the applied potential. Thus, the plot of −(kT/e) log*k* vs. *E* is roughly linear, and its slope yields a charge-transfer coefficient $\alpha = 0.75$ (data not shown).

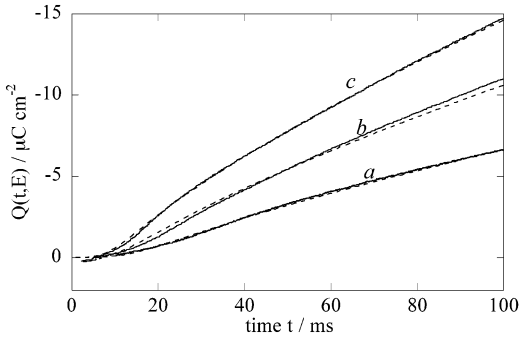

Figure 9. Solid curves are *Q(t,E)* vs *t* plots for the electroreduction of 1 × 10^{-4} M Tl^+ in aqueous 0.1 M KCl on a mercury electrode coated with a (67 mol % DOPC+33 mol % KC) monolayer at $E = -0.580$ (a), −0.590 (b), and −0.600 V (c). The parameters employed for the calculation of the surface coverage $p\theta_0 S(t,p)$ are reported in Figure 6. The rate constant *k* for the charge-transfer step is given values 5.5 × 10^{-3} (a), 8 × 10^{-3} (b), and 1 × 10^{-2} cm/s (*c*).

Disruption of the KC Pores. The kinetic process of pore disruption can be treated as a nucleation and growth of holes within the surface area covered by the KC clusters. By nucleation of holes we mean the quasi-reversible detachment of an initial number of KC molecules from a cluster and their random intercalation with the DOPC molecules. By growth of holes, we mean the subsequent irreversible detachment of the remaining KC molecules from the cluster, leading to its complete disruption. At potentials just preceding pore disruption, all initial random monomers of fractional surface coverage θ_0 are present in the form of clusters. Consequently, the surface coverage by clusters just before pore disruption occurs is equal to θ_0. Let us denote by S_h the ratio of the area actually covered by holes (i.e., by the random KC monomers being released by the clusters) over that, θ_0, initially covered by clusters. Since the nucleation of holes takes place within the surface area covered by clusters, the nucleation rate $v_{h,N}$ will be set proportional to this fractional surface area, $\theta_0(1-S_h)$, according to a proportionality constant $k_{h,N}$. It will also be regarded as independent of the applied potential. During the initial growth of a hole in a cluster, the hole will be in contact with KC molecules participating in the given cluster. Therefore, in view of eq 2, the rate $v_{h,R}$ of radial growth will be regarded as roughly independent of the surface coverage by clusters. On the other hand, it will be considered to increase as the applied potential is made progressively more negative, thus favoring the detachment of KC molecules from the clusters.

The experimental *Q(t,E)* vs *t* curves relative to the second 2D phase transition, corrected for the capacitive charge passed before the phase transition occurs by a procedure analogous to that adopted for the curves in Figure 8, are shown by the solid curves in Figure 10. They must be compared with the curves of $\Delta'\sigma_M\theta_0 S_h$ vs *t* (dashed curves in Figure 10), where $\Delta'\sigma_M$ is the change in charge density on the metal in passing from the clusters to the monomers resulting from their disruption, while

(41) Delahay, P.; Strassner, J. E. *J. Am. Chem. Soc.* **1951**, *73*, 5219−5222.

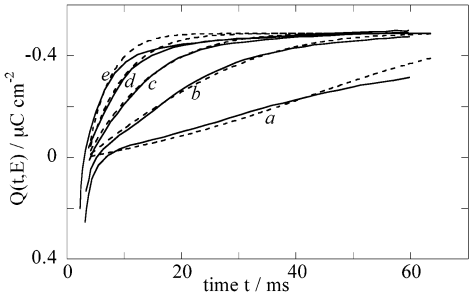

Figure 10. Solid curves are $Q(t,E)$ vs E plots for the second 2D phase transition of a (67 mol % DOPC+33 mol % KC) monolayer self-assembled on mercury, corrected for the capacitive charge passed before the phase transition takes place. E values: −0.690 (a), −0.700 (b), −0.710 (c), −0.720 (d), and −0.730 V(e).The dashed curves were calculated for $\theta_0 = 0.33$, $\Delta'\sigma_M = -1.48$ μC cm^{-2} and for $k_{h,N}{}^{1/2}\upsilon_{h,R} = 126$ (a), 252 (b), 378 (c), 505 (d), and 631 s$^{-3/2}$ (e).

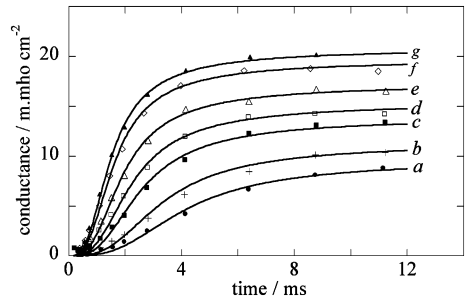

Figure 11. Markers are conductance values in squid giant axon at 6−7 °C (Hodgkin and Huxley, 1952) brought about by the following depolarizations: 32 (a), 38 (b), 51 (c), 63 (d), 76 (*e*), 88 (f), and 100 mV (g). The solid curves were calculated for $\theta_0 = 0.03$, $n = 2$, $k_N{}^{1/2}k_R = 1.95 \times 10^7$ s$^{-3/2}$, $p = 0.47$ (a), 0.55 (b), 0.67 (c), 0.74 (d), 0.83 (e), 0.946 (f), and 1 (g) and for a normalizing factor of 697 m.mho cm^{-2}.

$\theta_0 S_h$ is the fractional surface coverage by these monomers. Agreement between experimental and calculated curves is good. The $\upsilon_{h,R}$ values that provide the best fit vary exponentially with the applied potential. Thus, the plot of $-(kT/e)$ ln $\upsilon_{h,R}$ vs E is roughly linear, with a slope equal to $\alpha' = 1.17$ (data not shown). Here, $\alpha' eE$ can be tentatively regarded as the work that the interfacial electric field does against the electrostatic attraction between the KC dipoles and the K^+ ions present in the polar-head region, causing the resulting electrostatic repulsion between the neighboring and equally oriented KC dipoles to move them apart up to pore disruption.

Implication of the Model for Biological Voltage-Dependent Conductance. The present model of nucleation and growth is entirely general. Thus, it only assumes that the elementary steps preceding the step yielding the nucleus are in quasi-equilibrium, and that the cluster growth beyond the nucleus proceeds irreversibly by activated aggregation of monomers to the growing cluster. It is, therefore, of interest to verify whether it can also be applied to more familiar channels yielding sigmoidal voltage-clamp curves, such as the potassium channels investigated by Hodgkin and Huxley[1]. K channels consist of four independent and identical subunits that aggregate to form a unitary structure with the transmembrane pore passing through the middle.

Figure 11 shows the experimental points of the Hodgkin−Huxley (HH) conductance vs time curves of potassium channels of the squid giant axon at 6−7 °C at different depolarization potentials[1]. The solid curves were calculated by setting the fractional surface coverage θ_0 by the subunits equal to 0.03. This is a reasonable value in view of an estimated surface density of 320 μm^{-1} for the K channels in the squid giant axon[42] and of a surface area of about 100 nm^2 for Shaker K channels.[43] The best fit was obtained by setting the number n of subunits forming a nucleus equal to 2 and the product $k_R\, k_N{}^{1/2}$ accounting for the kinetics of nucleation and growth equal to 1.95×10^7 s$^{-3/2}$. As distinct from the fitting to the experimental charge vs potential curves in Figure 8, where the normalizing factor of the area $p\theta_0 S(t,p)$ covered by the growing clusters is the gating charge, in the present case the normalizing factor g has the dimensions of a channel conductance. In fact, $p\theta_0 S(t,p)$ is now a measure of the density of open K channels. The fitting is extremely good, and accounts for the slow initial delay and the maximum slope of the experimental curves better than the empirical kinetic equations of the HH model. Moreover, the fitting relies on only two potential-independent free parameters, namely n and $k_R\, k_N{}^{1/2}$. The potential dependence is expressed exclusively by a probability factor p that satisfies the Boltzmann equation. This is to be expected because the probability p is practically equal to the ratio of the steady-state conductance to its maximum limiting value, which exhibits the same Boltzmann behavior in the HH model. The number of free parameters used in the present model is low when we consider that the HH model uses five free parameters to express the potential dependence of the a_n and b_n quantities employed to fit the voltage-clamp curves. By setting $n = 3$ the best fit to the experimental points in Figure 11 is obtained with $k_R k_N{}^{1/2} = 1.16 \times 10^8$ s$^{-3/2}$. However, this fit is slightly worse than that in Figure 11, because the initial delay is too pronounced, especially at the lower depolarization potentials.

A major difference between the present model and recent refined models of K channels[44−46] is represented by the assumption of an aggregation of subunits controlled by nucleation-and-growth kinetics. Even though no evidence exists at present that the subunits of K channels can dissociate spontaneously after assembly, the model accounts quite satisfactorily for all detailed features of the voltage-clamp curves, including the initial delay. It must be stressed that nucleation-and-growth kinetics by no means implies a diffusion of the subunits toward each other, but rather the assumption that a potential-induced reorientation or conformational change of the subunits may first give rise to the formation of a nucleus of n subunits; the arrangement of these n subunits, favorable to channel formation, will then make the proper arrangement of the remaining subunits easier during the irreversible growth stage. In other words, a positive cooperativity between the subunits forming the channel is postulated. An increasing cooperativity is opposite to what predicted by the HH model. However, it has been recently shown that the on and off gating currents for noninactivating mutants of Shaker K channels show a complex time course, with an initial rising phase and multiple time constants, which is only compatible with an increasing cooperativity in opening.[45] The present model, in which the progressive clustering of subunits involved in the nucleation-and-growth process is assumed to run in parallel with the resulting K current, also

(42) Conti, F.; De Felice, L. J.; Wanke, E. *J. Physiol.* **1975**, *248*, 45−82.
(43) Sokolova, O.; Kolmakova-Partensky, L.; Grigorieff, N. *Structure* **2001**, *9*, 215−220.
(44) Zagotta, W. N.; Hoshi, T.; Aldrich, R. W. *J. Gen. Physiol.* **1994**, *103*, 321−362.
(45) Rodriguez, B. M.; Sigg, D.; Bezanilla, F. *J. Gen. Physiol.* **1998**, *112*, 223−242.
(46) Zheng, J.; Sigworth, F. J. *J. Gen. Physiol.* **1998**, *112*, 457−474.

implies the existence of conductance substates. These may be interpreted as partially blocked open channels, in which only a few rather than all the component subunits have attained the proper channel-forming conformation. This conclusion does not violate the idea of a single normal open state.[47] Even though many kinetic models in the literature describe the open channel as a single kinetic state, this assumption is unnecessarily restrictive. Thus, for example, it was recently found that Shaker K channels with removed inactivation open and close through a quick staircase of conductance channels.[46,48]

As early as 1952, Hodgkin and Huxley[1] pointed out that the inability of their model to account exactly for the initial delay in the voltage-clamp curves of K channels might be overcome with a fifth or sixth power of their probability factor *n*. Recent refined kinetic models have actually introduced several gating steps,[44,46,48] thus accounting satisfactorily for macroscopic current, single-channel current and gating current of Shaker K channels with removed inactivation. The present model, while accounting quite satisfactorily for such an initial delay in macroscopic current, is too general to enter into the details of all features of K channels. More precisely, it says nothing about the possible causes of the voltage-dependent probability *p* of the subunits of the homomeric tetramer being in the proper conformation. However, it shows that, once these causes are suitably modeled, the detailed features of the voltage-clamp curves of K channels can be conveniently accounted for with a minimum of free voltage-independent parameters on the basis of nucleation-and-growth kinetics. It is also possible that certain sigmoidal voltage-clamp curves such as those reported for the channel-forming peptide monazomycin,[3−5] which were interpreted on the basis of an auto-catalytic process, may be equally well explained by nucleation-and-growth kinetics.

Appendix

Differentiating S_x in eq 5 with respect to *t* via the generalized Leibnitz formula while taking eq 2 into account we obtain

$$dS_x/dt = 2\pi k_R p\theta(t)u(t) \quad with{:}u(t) \equiv \int_0^t R(t,y)\upsilon_N(y)dy \quad \text{(A1)}$$

Differentiating $u(t)$ with respect to *t* yields

$$du/dt \equiv k_R p\theta(t)q(t) \quad with{:}q(t) \equiv \int_0^t \upsilon_N(y)dy \quad \text{(A2)}$$

Finally, differentiating $q(t)$ with respect to *t* and taking eq 1 into account we obtain

$$dq/dt = \upsilon_N(t) = k_N p^n \theta^n \quad \text{(A3)}$$

The ratio $S(t,p)$ of the area covered by the growing clusters over that initially covered by the favorably oriented monomers is obtained by solving the system of the four differential eqs 6, A1, A2 and A3 by the fourth-order Runge−Kutta method with the initial conditions $\theta = \theta_0$ and S_x, S, u, and q equal to zero.

The disruption of pores by nucleation and growth of holes in the preformed clusters is treated by an analogous procedure. Let us denote by $S_{h,x}$ the hypothetical area covered by the holes (i.e., the random monomers resulting from the progressive disruption of clusters) over that initially covered by the clusters upon neglecting overlapping of holes. In analogy with eq 5, $S_{h,x}$ is given by

$$S_{h,x} = \pi\int_0^t [\int_y^t \upsilon_{h,R}(z)dz]^2 \upsilon_{h,N}(y)dy \quad \text{(A4)}$$

where $\upsilon_{h,N}$ and $\upsilon_{h,R}$ denote the rates of nucleation and of radial growth of the holes. Differentiation of $S_{h,x}$ with respect to time under the assumption that $\upsilon_{h,R}$ is time-independent yields

$$dS_{h,x}/dt = 2\pi\upsilon_{h,R}{}^2 u_h(t) \quad with{:}u_h(t) \equiv \int_0^t \upsilon_{h,N}(y)(t-y)dy \quad \text{(A5)}$$

Differentiating $u_h(t)$ yields:

$$du_h/dt = q_h \quad with{:}q_h \equiv \int_0^t \upsilon_{h,N}(y)dy \quad \text{(A6)}$$

Finally, upon differentiating q_h we get

$$dq_h/dt = \upsilon_{h,N}(t) = k_{h,N}\theta_0(1 - S_h) \quad \text{(A7)}$$

The relation between $S_{h,x}$ and S_h is again expressed by Avrami's equation (eq 6)

$$dS_h/dt = (1 - S_h)dS_{h,x}/dt \quad \text{(A8)}$$

The system of the four differential equations (A5)−(A8) is solved by the fourth-order Runge−Kutta method.

Acknowledgment. The financial support of the Ministero dell'Istruzione, dell'Universitá e della Ricerca of Italy and of the Ente Cassa di Risparmio di Firenze are gratefully acknowledged.

JA029428J

(47) Hille B. *Ion channels of Excitable Membranes*, 3rd ed. Sinauer Associates, Inc. Sunderland: MA, 2001; p 600.
(48) Zheng, J.; Sigworth, F. J. *J. Gen. Physiol.* **1997**, *110*, 101−117.